

An HI study of three long-tailed irregular galaxies in the cluster Abell 1367

Ananda Hota^{1,2,3*} and D.J. Saikia^{2 †}

¹ *Academia Sinica Institute of Astronomy and Astrophysics, P.O. Box 23-141, Taipei 10617, Taiwan, Republic of China*

² *National Centre for Radio Astrophysics (TIFR), Ganeshkhind, Pune 411 007, India*

³ *JAP Program, Indian Institute of Science, Bangalore 560 012, India*

Received 26 March 2007; accepted 31 May 2007

Abstract. We present the results on the distribution and kinematics of HI gas with higher sensitivity and in one case of higher spectral resolution as well than reported earlier, of three irregular galaxies CGCG 097073, 097079 and 097087 (UGC 06697) in the cluster Abell 1367. These galaxies are known to exhibit long (50–75 kpc) tails of radio continuum and optical emission lines (H α) pointing away from the cluster centre and arcs of starformation on the opposite sides of the tails. These features as well as the HI properties, with two of the galaxies (CGCG 097073 and 097079) exhibiting sharper gradients in HI intensity on the side of the tails, are consistent with the HI gas being affected by the ram pressure of the intracluster medium. However the HI emission in all the three galaxies extends to much smaller distances than the radio-continuum and H α tails, and are possibly still bound to the parent galaxies. Approximately 20–30 per cent of the HI mass is seen to accumulate on the downstream side due to the effects of ram pressure.

Keywords : galaxies: individual: CGCG 097073, CGCG 097079 and CGCG 097087 (UGC 06697) – galaxies: interaction – galaxies: ISM – galaxies: kinematics and dynamics

*e-mail: hota@asiaa.sinica.edu.tw

†e-mail: djs@ncra.tifr.res.in

Table 1. Basic data on these three galaxies.^a

Galaxy ^a	RA ^b	Dec ^b	Type ^c	a×b ^d	V _{sys} ^e	D ^f	S _{HI} ^g	S ^h
CGCG	h m s	° ' "		' × '	km /s	Mpc	Jy km/s	mJy
097073	11 42 56.4	+19 57 58	SACd, pec	0.5×0.5	7275±6	86	1.0	25
097079	11 43 13.4	+20 00 17	Irr	0.5×0.4	7000±9	86	0.8	15
097087	11 43 49.1	+19 58 06	Im	1.9×0.3	6725±2	86	3.5	60

^a Taken from the NASA Extragalactic Database (NED), unless stated otherwise.

^b Optical position of the galaxy from NED in J2000 co-ordinates.

^c Morphological type.

^d Optical major and minor axes.

^e Heliocentric systemic velocity.

^f Assumed distance to the object from Gavazzi et al. (2001b). For this distance 1''=417 pc.

^g Total HI line flux density taken from Arecibo measurements by Gavazzi (1989).

^h Total 1.4 GHz radio continuum flux density from the VLA D-array observations of Gavazzi (1989).

1. Introduction

Clusters of galaxies, which are the most massive gravitationally bound systems in the Universe, provide us with an opportunity to study the effects of the local environment on the structure, evolution and star formation history of its constituent galaxies (e.g. Gunn & Gott 1972; Dressler 1980; Boselli & Gavazzi 2006). Besides interactions with neighbouring galaxies, the hot intracluster medium (ICM) is also likely to play an important role in influencing the observed properties of the galaxies. Simulations of stripping and compression of gas in spirals falling into a cluster by the ram pressure of the ICM have shown this to have a range of manifestations (Abadi, Moore & Bower 1999; Quilis, Moore & Bower 2000; Vollmer et al. 2001; Schulz & Struck 2001; Bekki & Couch 2003; Roediger & Brüggén 2006). For example, while the galactic interstellar medium (ISM) may be largely stripped in a high ICM density region leading to a suppression of star formation, the star formation rate may be enhanced in a less dense ICM region where the ISM is only compressed rather than being completely stripped. In addition to these effects, clusters of galaxies also provide us with important insights towards understanding the formation of large-scale structures in the Universe (e.g. West, Villumsen & Dekel 1991; Katz & White 1993). Many of these clusters have sub-structures, suggesting that these are dynamically young systems still in the process of formation.

The cluster Abell 1367 is an interesting nearby system at a distance of ~ 86 Mpc where three subgroups containing a number of star-forming galaxies are falling into the core of the cluster (see Cortese et al. 2004). The cluster lies at the intersection of two filaments and has been suggested to be a prototype of a dynamically young cluster (e.g. Cortese et al. 2004, 2006). Optical and radio observations of individual galaxies by Gavazzi et

al. (1995, 2001a,b) also suggest infall of galaxies into the cluster core. Gavazzi & Jaffe (1987) reported the discovery of extended tails of radio continuum emission associated with three irregular galaxies in the north-west region of A1367, namely CGCG 097073, 097079 and 097087 (UGC 06697). Tails of H α emission associated with the radio tails have also been reported by Gavazzi et al. (1984; 2001a,b). X-ray observations of UGC 06697 also suggest that interaction between the ISM and ICM plays a major role in the observed structures (Sun & Vikhlinin 2005). We have listed the basic properties of these three galaxies in Table 1. All the three galaxies have an asymmetric radio structure with a ‘head’ in the up-stream side roughly towards the cluster centre and a ‘tail’ on the opposite down-stream side with the size of the radio emission exceeding the size of the optical galaxy (e.g. Gavazzi 1978; Gavazzi & Jaffe 1987). The galaxies CGCG 097073 and 097079 also exhibit an arc of HII regions suggesting star formation on their leading edges approximately towards the cluster centre (Gavazzi et al. 1995, 2001a,b). These features are consistent with the paradigm where ram pressure due to the ICM is significantly affecting the observed properties of the galaxies. Observations of the atomic HI gas are also consistent with the ram pressure paradigm. Gavazzi (1989) found the galaxies to be deficient in HI compared with field galaxies from observations with the Arecibo telescope. The reported interferometric observations of HI which only plotted the locations of the peaks of emission in a few channels showed the gas to be displaced in the direction of the radio tails (Gavazzi 1989; Dickey & Gavazzi 1991; hereafter referred to as DG91), while the molecular gas content of the galaxies appeared to be normal with the distribution exhibiting no strong asymmetries (Boselli et al. 1994).

In this paper we present the detailed distribution and velocity field of HI gas in all the three galaxies, CGCG 097073, 097079 and 097087 (UGC 06697), with better sensitivity and in one case, CGCG 097079, with higher spectral resolution as well, using archival Very Large Array (VLA) data with both the C- and D-configurations. These data were also reduced with the objective of trying to detect any HI gas from the long tails seen at other wavelengths. In this context it is relevant to note that Oosterloo & van Gorkom (2005) have reported the detection of an HI tail ~ 110 kpc long which has been formed by gas stripped from the galaxy NGC4388 by ram pressure. The extent of the tail suggests that gas could remain neutral for $\sim 10^8$ yr in the intracluster medium. A similar feature of ~ 75 kpc in length near the galaxy NGC4438 has been reported by Hota, Saikia & Irwin (2007), but it is possible that this feature may also be of Galactic origin. Although the observations of CGCG 097073, 097079 and 097087 (UGC 06697) reported here do not reveal long HI tails, they reveal new features which we compare with observations at other wavelengths and simulations of ram pressure stripping.

2. Observations and data analysis

The observing log for the observations is presented in Table 2, which is arranged as follows. Column 1: name of the telescope where we list the configuration for the observations. The program code for the observations in 1988 is AG264 (Principal investigator: J. Dickey,

Table 2. H I Observation log

Telescope Array (1)	Observation date (2)	Time hrs (3)	Channel separation kHz, km/s (4)	Band width MHz, km/s (5)
VLA-D	26 March 1999	9	98, 22	3.1, 650
VLA-C	02 April 1988	8	391, 86	12.5, 2600
VLA-D	25 July 1988	3	391, 86	12.5, 2600

DG91) while for those in 1999 it is AB900 (Principal investigator: B. Burke). Columns 2 and 3: dates of the observations and the time, t , spent on the source in hours; column 4: the channel separation in units of kHz and km s^{-1} ; column 5: the bandwidth of the observations in units of MHz and km s^{-1} .

The observations were made in the standard fashion, with each source observation interspersed with observations of the phase calibrator. The primary flux density and bandpass calibrator was 3C286 whose flux density was estimated on the Baars et al. (1977) scale using the 1999.2 VLA values. The data analysis was done using the Astronomical Image Processing System (AIPS) of the National Radio Astronomy Observatory. The AIPS task UVLIN was used for continuum subtraction and the multi-channel data were then CLEANed using IMAGR.

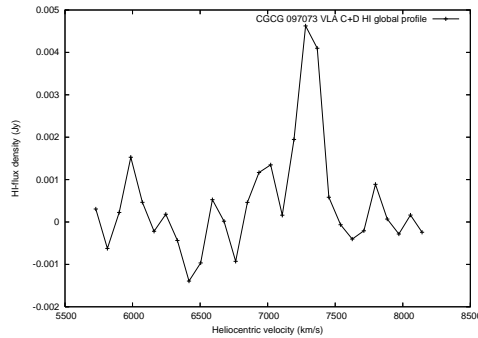


Figure 1. CGCG 097073: H I global profile of the galaxy observed with a spatial and spectral resolution of $\sim 21''$ and 86 km s^{-1} respectively.

3. Observational results

The VLA C- and D-array data which has a velocity resolution of 86 km s^{-1} were combined to create a data cube with a spatial resolution of $\sim 21''$ for all the three galaxies,

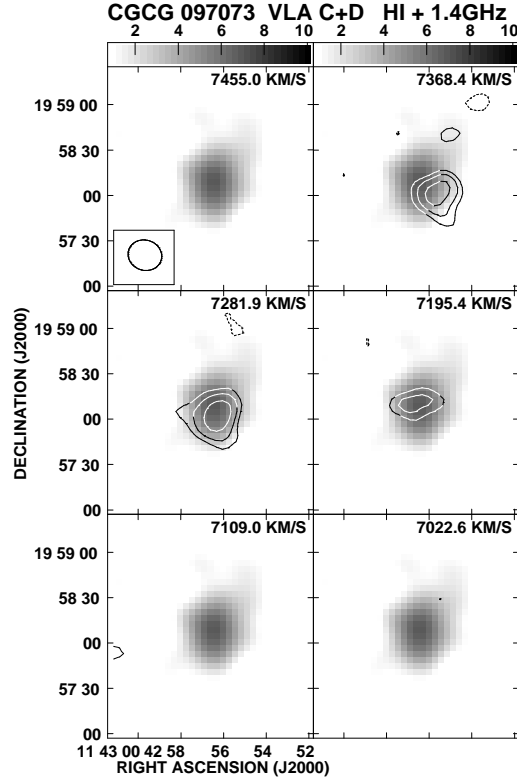


Figure 2. CGCG 097073: The HI channel maps in contours have been superimposed on the gray scale single channel continuum image obtained from the same data with a resolution of $\sim 21''$. The contour levels are $0.3 \times (-4, -2.82, 2.820, 4, 5.65 \dots)$ mJy/beam.

while the VLA D-array data with a velocity resolution of 22 km s^{-1} was used to image the galaxy CGCG 097079. The observational parameters and some results from the HI images are presented in Table 3 which is arranged as follows. Columns 1 and 2: the configuration of the VLA observations and the spectral resolution in units of km s^{-1} ; columns 3, 4 and 5: the major and minor axes of the restoring beam in arcsec and its position angle in deg.; columns 6 and 7: the rms noise in the image and the spectrum in units of mJy/beam and mJy respectively; columns 8, 9 and 10: the total HI flux density in units of Jy km s^{-1} for the galaxies CGCG 097073, 097079 and 097087 respectively.

Table 3. Observational parameters and some results from the HI images

VLA	Vel	Beam size			map	spec.	S_{HI}	S_{HI}	S_{HI}
	res.	maj.	min.	PA	rms	rms	(097073)	(097079)	(097087)
	km	"	"	°	mJy	mJy	Jy	Jy	Jy
	/s				/b		km/s	km/s	km/s
(1)	(2)	(3)	(4)	(5)	(6)	(7)	(8)	(9)	(10)
D	22	43.2	41.8	-51.3	0.33	0.4		0.38	
CD	86	22.5	19.9	71.8	0.30	0.7	0.92	0.52	2.67

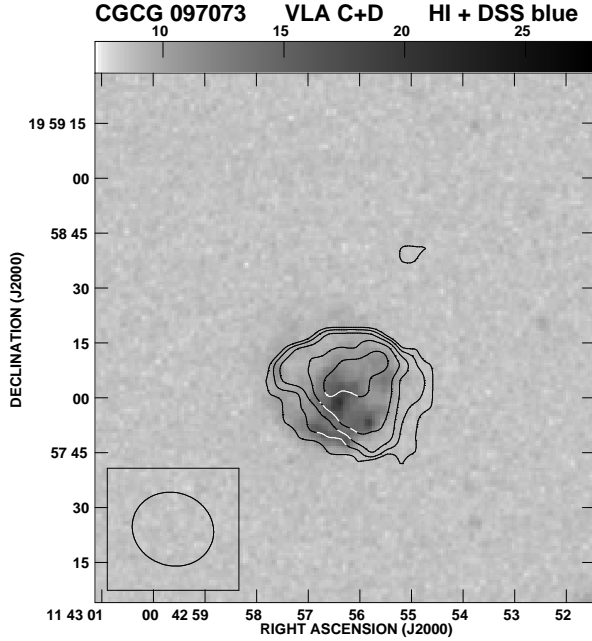


Figure 3. CGCG 097073: Total intensity HI contour map with a resolution of $\sim 21''$ has been superimposed on the DSS blue-band image. The contour levels are 2.358×10^{20} atoms cm^{-2} or $1.89 M_{\odot} \text{pc}^{-2}$ and then increasing in steps of $\sqrt{2}$.

3.1 CGCG 097073

The global profile obtained from the combined VLA C- and D-array data with a spatial resolution of $\sim 21''$ and a velocity resolution of 86 km s^{-1} does not show any significant asymmetry, consistent with the spectrum obtained with the Arecibo telescope (Gavazzi 1989). Significant emission is seen in three channels whose velocities cover a range of

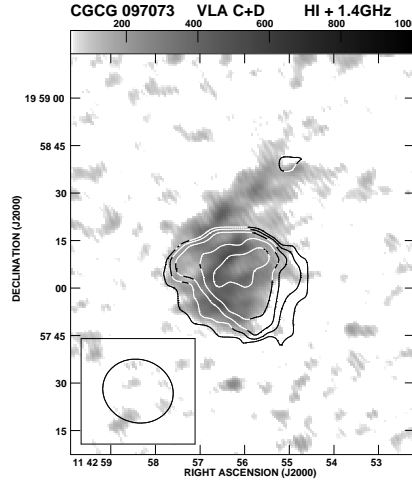


Figure 4. CGCG 097073: Same HI map on the 1.4-GHz radio continuum image made with a resolution of $\sim 4''$. The contour levels are 2.358×10^{20} atoms cm^{-2} or $1.89 M_{\odot} \text{pc}^{-2}$ and then increasing in of $\sqrt{2}$.

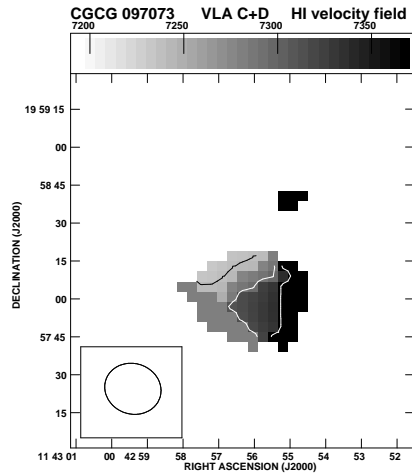


Figure 5. CGCG 097073: The intensity weighted HI velocity field made from the same image cube with a spatial and spectral resolution of $\sim 21''$ and 86 km s^{-1} respectively. The contours are 7240 , 7300 and 7360 km s^{-1} from east to west.

$\sim 200 \text{ km s}^{-1}$. The width of the HI spectrum obtained with the Arecibo telescope is 294 km s^{-1} . Both these values are significantly larger than the velocity width of 85 km s^{-1}

estimated from the Tully Fisher relation and inclination of the optical disk by Gavazzi (1989), suggesting strong kinematic effects leading to non-circular motions in the ISM. The total HI mass estimated from the global profile is $1.6 \times 10^9 M_{\odot}$. The peak of the HI emission is consistent with the optical systemic velocity of 7225 km s^{-1} . The HI emission channel maps in contours are shown superimposed on the radio-continuum, single channel gray scale image in Fig. 2. It is clear that the position of the peak of HI emission varies from channel to channel. DG91 reported HI emission at 7282 and 7196 km s^{-1} with the lower velocity detection towards the northern edge of the optical image. We clearly see these two features but also emission at 7368 km s^{-1} towards the south-western part of the optical image. We have not been able to confirm the possible weak component towards the north-west with a velocity of 7109 km s^{-1} noted by DG91.

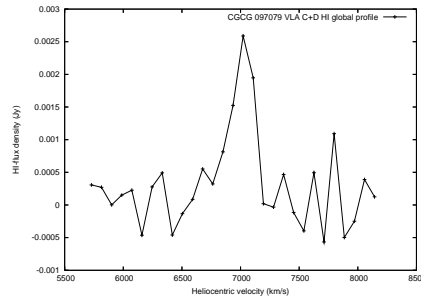


Figure 6. CGCG 097079: Global HI profile of the galaxy made with a spatial and spectral resolution of $\sim 21''$ and 86 km s^{-1} respectively.

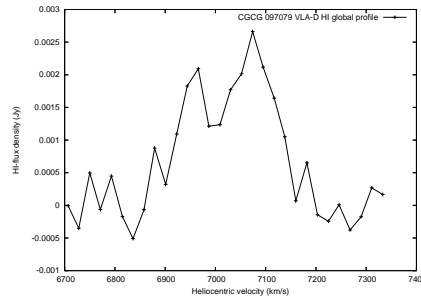


Figure 7. CGCG 097079: Global HI profile of the same galaxy made with a spatial and spectral resolution of $\sim 42''$ and 22 km s^{-1} respectively.

A moment map generated from these three channels with a 3σ cut off is presented in Fig. 3. The total intensity HI (moment 0) map is shown superimposed on the DSS blue-band optical image of the galaxy. On the southern edge of the optical disk the stellar arc is visible with the HI contours having a relatively sharper edge on the northern side. This

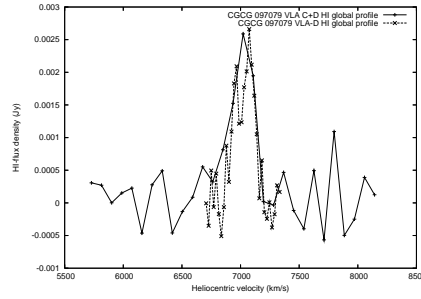


Figure 8. CGCG 097079: Global HI profiles from the earlier two figures plotted together.

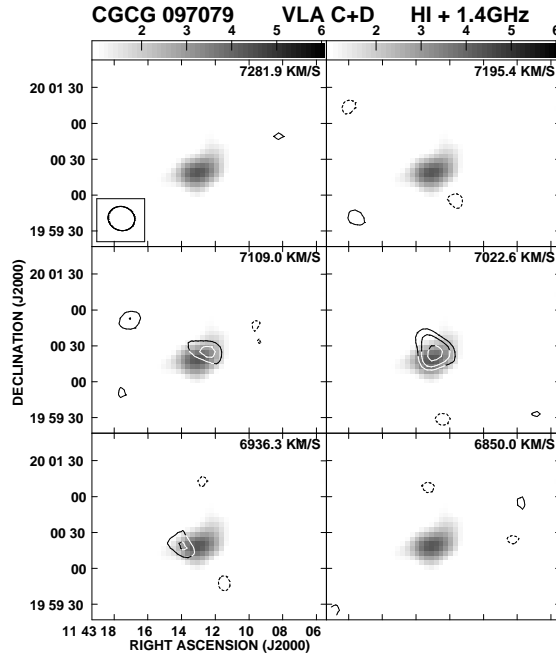


Figure 9. CGCG 097079: The HI channel maps in contours have been superimposed on the gray scale single channel continuum image obtained from the same data with a resolution of $\sim 21''$. The contour levels are $0.3 \times (-4, -2.82, 2.820, 4, 5.65 \dots)$ mJy/beam.

sharper HI contours on the opposite side of the optical starforming arc is also visible in the galaxy NGC2805, a member of the group Ho 124 (Bosma et al. 1980; Kantharia et al. 2005). Coincidentally NGC2805 is also seen nearly face on and the galaxies in that group

show evidence of ram pressure stripping and galaxy interactions. The accumulation of gas in the down-stream region can be qualitatively understood as being due to the effect of ram pressure on the rotating gas. The rotating gas following the ram pressure will reach the down-stream region faster while the gas rotating against the ram pressure direction will face a greater resistance and thus spending a longer time on the down-stream region. Due to ram pressure one would also expect the up-stream side to get compressed and trigger star formation. Although at optical wavelengths there is an arc of HII regions possibly triggered by compression of gas due to ram pressure, the HI intensity contours do not appear to be particularly edge-brightened.

The moment 0 image is also shown superimposed on a radio-continuum image at 1.4 GHz with an angular resolution of $\sim 4''$ made from archival VLA AB-array data (Fig. 4). At this resolution there is no clearly defined peak of radio continuum emission. The southern arc-shaped region seen in radio continuum is also slightly offset from the southern most peak of the arc seen at optical wavelengths. Although this higher resolution image shows the orientation of the tail to the north-west, a larger-scale image with lower angular resolution shows that the tail extends almost to the north (Gavazzi & Jaffe 1987). We can see that on the northern side there is no correspondence of the HI and radio continuum emission in the tail. Hence it is possible that we do not detect HI from the stripped tail but the HI gas is still largely rotating about the centre of the galaxy. Although the moment-one image shows evidence of rotation (Fig. 5), observations of higher spectral resolution are required to determine the velocity field.

3.2 CGCG 097079

The global profiles of HI emission made from the combined VLA C-and D-array data with a spectral resolution of $\sim 86 \text{ km s}^{-1}$ and the VLA D-array data with a spectral resolution of $\sim 22 \text{ km s}^{-1}$ are shown in Fig. 6, 7 and 8. The total mass estimated from the global spectra is $0.9 \times 10^9 M_{\odot}$. In Fig. 9 we present the higher spatial resolution channel maps showing the HI intensity superimposed on the single-channel radio-continuum image shown in gray scale. The HI emission is seen in three channels with velocities of 7109, 7023 and 6936 km s^{-1} with the emission peak shifting from north-west to south-east as we go lower in velocities. DG91 also reported HI at two velocities one having a peak to the north-west with a velocity of 7023 km s^{-1} and the other tentative detection on the western boundary of the optical disk at a velocity of 7109 km s^{-1} . We detect emission in a third channel at a velocity of 6936 km s^{-1} giving total velocity width of $\sim 260 \text{ km s}^{-1}$.

Moment maps were generated with a 3σ cutoff and only three channels with a clear detection were combined. A superposition of the the HI total-intensity contours on the DSS blue-band image (Fig. 10) show the south-eastern peak of HI emission to be coincident with the bright starforming region believed to be formed due to the ram pressure compression of the ISM. Most of the HI emission is on the north-western side of this peak, along a similar PA as that of the radio-continuum tail. A superposition of the contours

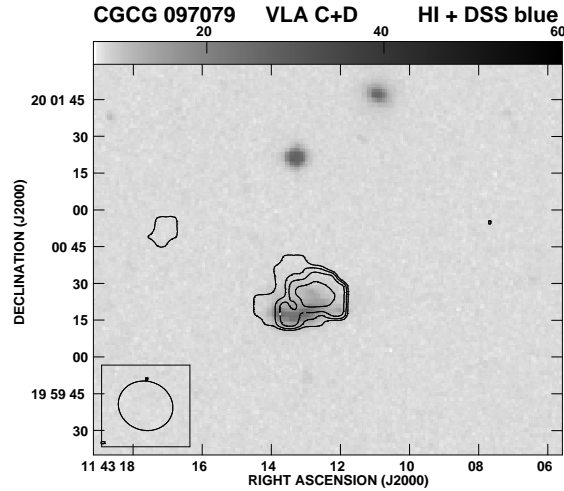


Figure 10. CGCG 097079: Total intensity HI contour map with a resolution of $\sim 21''$ has been superimposed on the DSS blue-band image. The contour levels are 2.358×10^{20} atoms cm^{-2} or $1.89 M_{\odot} \text{pc}^{-2}$ and then increasing in steps of $\sqrt{2}$.

of HI emission on a VLA B-array radio continuum image made from archival data with an angular resolution of $\sim 4''$ (Fig. 11) as well as comparison with the continuum image of Gavazzi et al. (1995) shows that the radio continuum emission extends well beyond the HI emission. There is a hint of sharper cut off of the HI contours on the western side which is again somewhat opposite to the arc of star formation, similar to the case of the face on galaxy CGCG 097073.

To examine the velocity field (Fig. 12) with higher spectral resolution we have reduced the VLA D-array data which has a spectral resolution of 22 km s^{-1} . The channel maps of the image cube with the contours of HI emission superposed on a single channel radio continuum image made from the same data using a line-free channel is shown in Fig. 13. Significant HI emission above a 3σ limit has been detected in nine channels with velocities ranging from 6923 to 7117 km s^{-1} giving a total width of $\sim 173 \text{ km s}^{-1}$. Because of the relatively poorer spatial resolution of ~ 45 arcsec the moment 0 image shows only a blob of emission with no evidence of any diffuse extended emission which may not have been seen in the higher-resolution image. Hence the moment maps are not presented here. However, to investigate the velocity field we have fitted a single Gaussian to HI emission in every channel whose position is marked with a + sign in Fig. 14. In this Figure the total intensity HI emission contours are superposed on an optical image of the galaxy

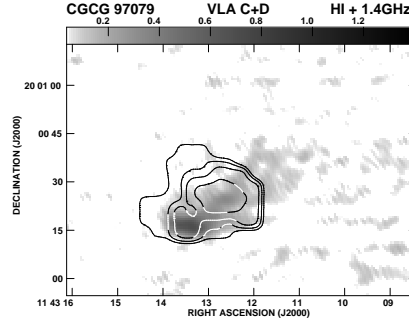


Figure 11. CGCG 97079: The same HI map superimposed on the 1.4-GHz radio continuum image made with a resolution of $\sim 4''$. The contour levels are 2.358×10^{20} atoms cm^{-2} or $1.89 M_{\odot} \text{pc}^{-2}$ and then increasing in steps of $\sqrt{2}$.

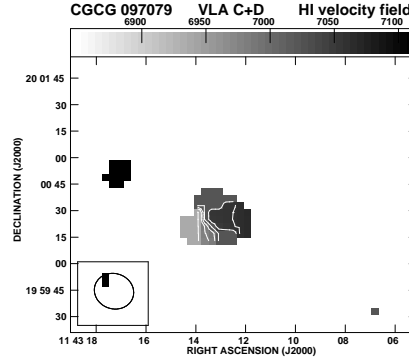


Figure 12. CGCG 97079: The intensity weighted HI velocity field made from the same image cube with a spatial and spectral resolution of $\sim 21''$ and 86 km s^{-1} respectively. The contours are 6940, 6980, 7000, 7020, 7040 and 7060 km s^{-1} from east to west

with the size of the + sign signifying the error in the fit. The velocity corresponding to each + sign is indicated in the Figure. The velocity of the extended emission on the north-western side has a velocity gradient which decreases from $\sim 7120 \text{ km s}^{-1}$ on its south-western side to $\sim 6920 \text{ km s}^{-1}$ on the north-eastern side, with the central velocity being close to the systemic velocity of the galaxy of $\sim 7000 \text{ km s}^{-1}$. The velocity of the HI gas close to the arc of star formation decreases from $\sim 7050 \text{ km s}^{-1}$ on the western side to $\sim 6950 \text{ km s}^{-1}$ on the eastern side. This shows that the gas in the disk as well

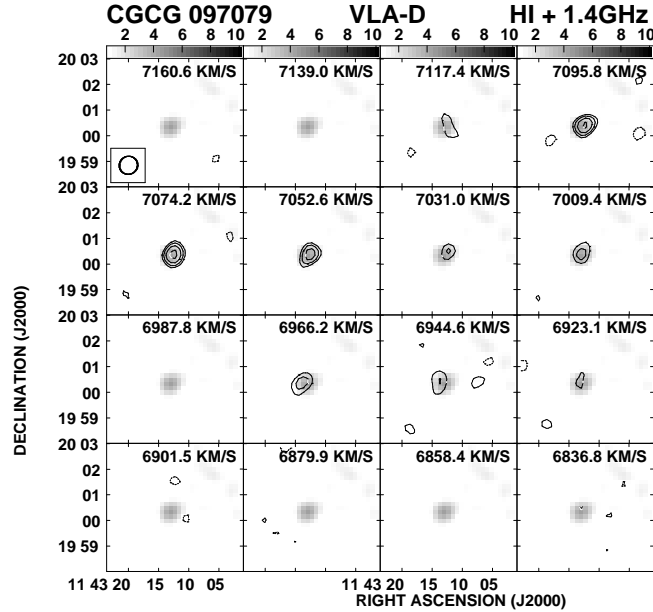


Figure 13. CGCG 097079: The HI channel maps in contours have been superimposed on the gray scale single-channel continuum image obtained from the same data with a spatial and spectral resolution of $\sim 42''$ and $\sim 22 \text{ km s}^{-1}$ respectively. The contour levels are $0.33 \times (-4, -2.82, 2.820, 4, 5.65 \dots)$ mJy/beam.

as the more extended extra-planar HI gas which has been affected by ram pressure due to the ICM have similar kinematic properties with a same sense of rotation. It is worth noting that Hota, Saikia & Irwin (2007) have found similar properties of the HI gas in the edge-on Virgo cluster galaxy NGC4438, where the elongated extra-planar gas has a similar sense of rotation as the HI gas in the disk of the galaxy.

3.3 CGCG 097087

In Fig. 15 we present the global HI profile of CGCG 097087 (UGC 06697) taken from the image cube which has a spatial and spectral resolution of $\sim 21''$ and 86 km s^{-1} respectively. The profile has a wide velocity width of $\sim 600 \text{ km s}^{-1}$ ranging from ~ 6435 to 7030 km s^{-1} , and is very much asymmetric with respect to the systemic velocity of 6725 km s^{-1} . There is more gas on the red-shifted side of the systemic velocity, the mass being $\sim 2.9 \times 10^9 M_{\odot}$ compared with $\sim 1.7 \times 10^9 M_{\odot}$ on the blue-shifted side. The spectrum is consistent with that obtained with the Arecibo telescope by Gavazzi (1989). The channel maps of HI

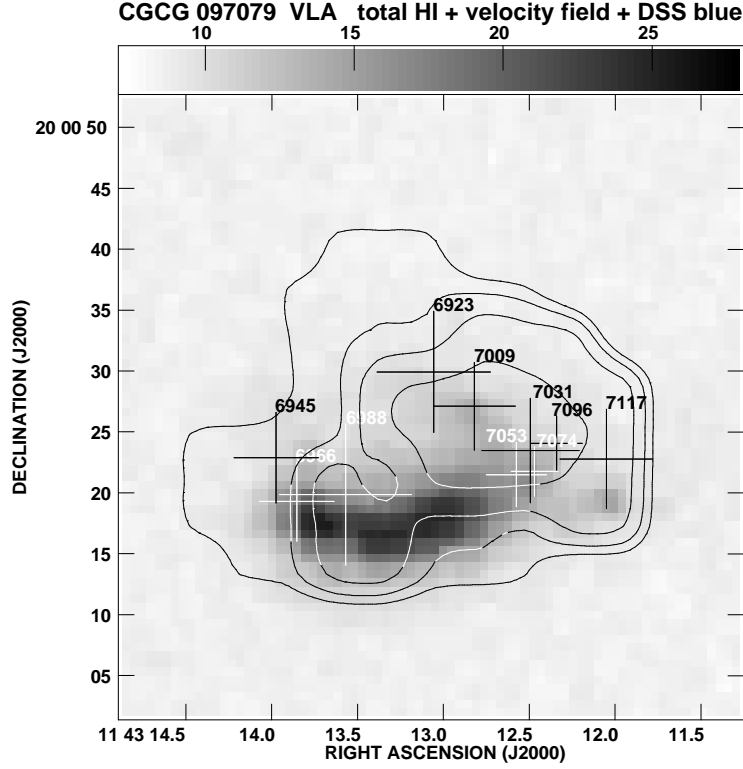


Figure 14. CGCG 097079: The higher spatial resolution total intensity HI contour of Fig. 10 has been superimposed on the DSS blue band image in gray scale. The '+' in the image marks the position of peak of the Gaussian fit to the higher spectral resolution single channel HI emission (Fig. 13). The size of the '+' gives the uncertainty in defining the peak. The corresponding heliocentric velocity of the higher spectral resolution channel emission has been marked close to the '+' mark. The contour levels are 2.358×10^{20} atoms cm^{-2} or $1.89 M_{\odot} \text{pc}^{-2}$ and then increasing in steps of $\sqrt{2}$. The diagonal velocity gradient and both the peaks of the HI emissions are clearly visible.

emission in contours superposed on a single-channel radio-continuum image in gray scale from a line free channel with the same resolution is presented in Fig. 16. The HI emission at higher velocities are seen towards the north-west while those with lower velocities are towards the south-east. DG91 reported detection in three velocity channels, namely at 6506, 6850 and 6936 km s^{-1} . Our recent re-analysis of the data shows emission in 8

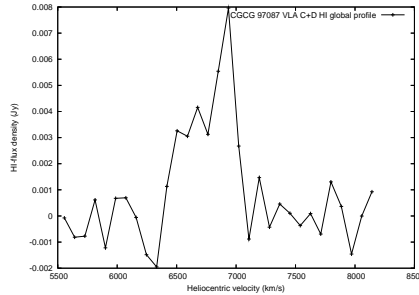


Figure 15. CGCG 097087: HI-global profile of the galaxy observed with a spatial and spectral resolution of $\sim 21''$ and 86 km s^{-1} respectively.

channels at $\geq 3\sigma$ level over a velocity range of $\sim 6420 \text{ km s}^{-1}$ to 7020 km s^{-1} spanning a range of $\sim 600 \text{ km s}^{-1}$.

We have generated the moment maps with a cut off at 3σ and shown the moment 0 image with the total-intensity HI emission contours superposed on the DSS blue-band optical image in Fig. 17. The total HI mass in the region of the bright optical disk of the galaxy is $\sim 1.4 \times 10^9 M_{\odot}$ compared with $\sim 3.2 \times 10^9 M_{\odot}$ for the blob of HI emission towards the north-west. The moment 0 image is shown superposed on the VLA B-array continuum image with an angular resolution of $\sim 4''$ made from archival VLA data (Fig. 18). The tails of radio continuum and HI emission are oriented along very similar PAs and appear to be of similar extents in this Figure. However, lower resolution images of the tail by Gavazzi & Jaffe (1987) show that the tail of radio continuum emission extends to $\sim 3'$ (75 kpc), much larger than the extent of HI emission which extend only up to 25 kpc from the centre of the galaxy (defined by the peak of the high resolution radio continuum observation).

The moment 1 map with the iso-velocity contours superposed on the HI total-intensity in gray scale is shown in Fig. 19. The HI emission coincident with the high-brightness optical disk shows evidence of solid body rotation, while the north-western region has a similar velocity of $\sim 6940 \text{ km s}^{-1}$.

4. Discussion and concluding remarks

HI observations of all the three galaxies CGCG 097073, 097079 and 097087 (UGC 06697) in the cluster Abell 1367 which have been presented here show the detailed distribution of the gas. Earlier HI observations of these galaxies with the VLA C- and D-arrays reported by Dickey & Gavazzi (1991) showed the location of a few regions of HI emission in different velocity channels. Our analysis of their data as well as more recent VLA D-array data with higher spectral resolution have revealed further details of distribution

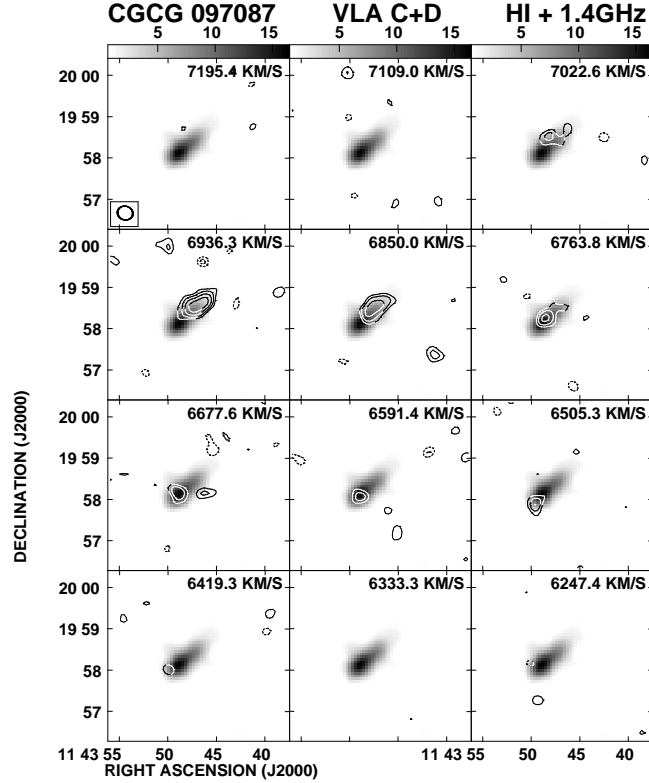


Figure 16. CGCG 097087: The HI channel maps in contours has been superimposed on the gray scale single channel continuum image obtained from the same data with a resolution of $\sim 21''$. The contour levels are $0.3 \times (-4, -2.82, 2.820, 4, 5.65 \dots)$ mJy/beam.

and kinematics of the HI gas. In all the three galaxies the mass of HI gas is $\sim 20\text{-}30\%$ larger on the down-stream side of the galaxies, showing that the distribution of the HI gas is affected by ram pressure of the ICM consistent with earlier suggestions (e.g DG91).

The directions of the tails of non-thermal radio continuum as well as $H\alpha$ emission suggest that CGCG 097073 is moving towards the south while CGCG 097079 is moving towards the south-east. In CGCG 097073 the HI gas appears to have a sharper gradient of the contours on the down-stream side roughly opposite to the arc of starformation region which is possibly caused by compression of gas due to the ram pressure of the ICM. There is a suggestion of a similar effect on the western side of CGCG 097079. The sharper gradient in the HI contours may be caused by the accumulation of gas in the down-stream side due to the effects of ram pressure. The total extent of the HI gas is ~ 8

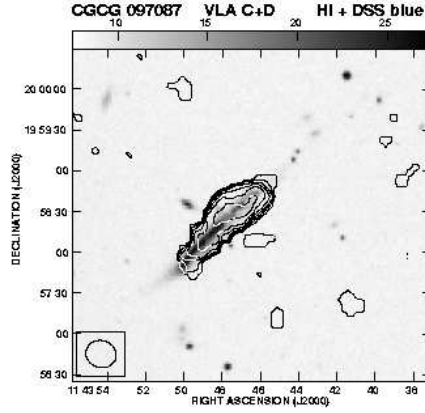


Figure 17. CGCG 097087: Total intensity HI contour map with a resolution of $\sim 21''$ has been superimposed on the DSS blue-band image. The contour levels are 2.358×10^{20} atoms cm^{-2} or $1.89 M_{\odot} \text{pc}^{-2}$ and then increasing in steps of $\sqrt{2}$.

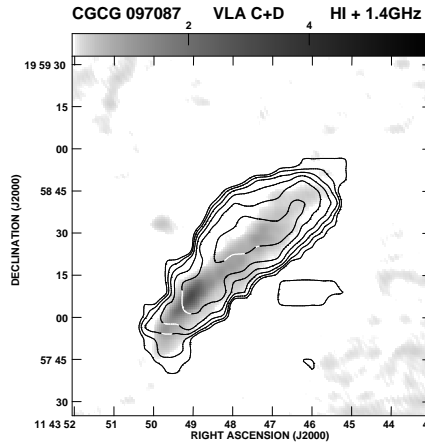


Figure 18. CGCG 097087: The same total intensity HI contours have been superimposed on the 1.4-GHz radio continuum image made with a higher resolution of $\sim 4''$. The contour levels are 2.358×10^{20} atoms cm^{-2} or $1.89 M_{\odot} \text{pc}^{-2}$ and then increasing in steps of $\sqrt{2}$.

kpc, 8 kpc and 37 kpc for CGCG 097073, 097079 and 097087 respectively, which is much smaller than the corresponding tails of non-thermal emission which extend for 75, 60 and 75 kpc respectively in the low-resolution images (Gavazzi & Jaffe 1987). The $H\alpha$ tails also extend for distances of 50, 75 and 55 kpc respectively which are also much larger than the regions of HI emission.

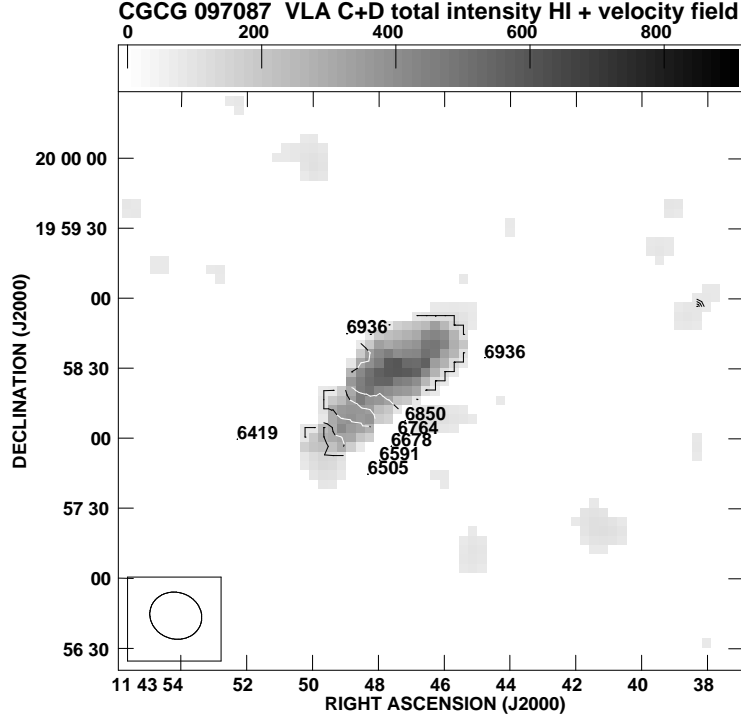


Figure 19. CGCG 097087: The intensity weighted HI velocity field has been superimposed on the gray scale image of the total intensity HI. The numbers close to the iso-velocity contours give the heliocentric velocity at intervals of the channel width of $\sim 86 \text{ km s}^{-1}$.

Results of three-dimensional numerical simulations of a spiral galaxy moving through a hot intracluster medium with its disk inclined at different angles to the direction of motion can produce a wide range of observed structures (e.g. Quilis, Moore & Bower 2000; Roediger & Brüggén 2006, and references therein). A comparison of the distribution and kinematics of the HI gas in CGCG 097079 with the results of these simulations shows that the gas in the disk of the galaxy is pushed backwards by the ram pressure of the ICM. The gas exhibits systematic rotation about the systemic velocity and is possibly still bound to the parent galaxy.

The direction of the radio tail in CGCG 097087 (UGC 06697) also suggests that this edge-on galaxy is moving towards the south-east. The HI observations show that while the gas associated with the higher brightness region of the optical galaxy exhibits solid-body rotation, most of the HI gas is pushed towards the north-west and has an almost constant velocity of $\sim 6940 \text{ km s}^{-1}$.

Acknowledgments

We thank the referee Dr G. Gavazzi for a very prompt and helpful report, Chanda Jog for discussions and K.S. Dwarakanath for his comments on an early version of this paper which has helped present the new results more clearly. VLA is operated by Associated Universities, Inc. under contract with the National Science Foundation. This research has made use of the NASA/IPAC extragalactic database (NED) which is operated by the Jet Propulsion Laboratory, Caltech, under contract with the National Aeronautics and Space Administration.

References

- Abadi M.G., Moore B., Bower R.G., 1999, MNRAS, 308, 947
 Baars J.W.M., Genzel R., Pauliny-Toth I.I.K., Witzel A., 1977, A&A, 61, 99
 Bekki K., Couch W.J., 2003, ApJ, 596, 13L
 Boselli A., Gavazzi G., 2006, PASP, 118, 517
 Boselli A., Gavazzi G., Combes F., Lequeux J., Casoli F., 1994, A&A, 285, 69
 Bosma A., Casini C., Heidmann J., van der Hulst J.M., van Woerden H., 1980, A&A, 89, 345
 Cortese L., Gavazzi G., Boselli A., Iglesias-Paramo J., Carrasco L., 2004, A&A, 425, 429
 Cortese L., Gavazzi G., Boselli A., Franzetti P., Kennicutt R.C., O'Neil K., Sakai S., 2006, A&A, 453, 847
 Dickey J.M., Gavazzi G., 1991, ApJ, 373, 347 (DG91)
 Dressler A., 1980, ApJ, 236, 351
 Gavazzi G., 1978, A&A, 69, 355
 Gavazzi G., 1989, ApJ, 346, 59
 Gavazzi G., Jaffe W., 1987, A&A, 186, 1L
 Gavazzi G., Tarengi M., Jaffe W., Boksenberg A., Butcher H., 1984, A&A, 137, 235
 Gavazzi G., Contursi A., Carrasco L., Boselli A., Kennicutt R., Scodreggio M., Jaffe W., 1995, A&A, 304, 325
 Gavazzi G., Marcelin M., Boselli A., Amram P., Vilchez J.M., Iglesias-Paramo J., Tarengi M., 2001a, A&A, 377, 745
 Gavazzi G., Boselli A., Mayer L., Iglesias-Paramo J., Vlchez J.M., Carrasco L., 2001b, ApJ, 563, 23L
 Gunn J.E., Gott J.R. III J., 1972, ApJ, 176, 1
 Hota A., Saikia D.J., Irwin J.A., 2007, MNRAS, in press (astro-ph/0706.3174)
 Kantharia N.G., Ananthakrishnan S., Nityananda R., Hota A., 2005, A&A, 435, 483
 Katz N., White S.D.M., 1993, ApJ, 412, 455
 Oosterloo T., van Gorkom J. 2005, A&A, 437, 19L
 Quilis V., Moore B., Bower R., 2000, Sci, 288, 1617
 Roediger E., Brüggem M., 2006, MNRAS, 369, 567
 Schulz S., Struck C., 2001, MNRAS, 328, 185
 Sun M., Vikhlinin A., 2005, ApJ, 621, 718
 Vollmer B., Cayatte V., Balkowski C., Duschl W.J., 2001, ApJ, 561, 708
 West M.J., Villumsen J.V., Dekel A., 1991, ApJ, 369, 287